HHS Public Access

Author manuscript

Biomacromolecules. Author manuscript; available in PMC 2024 May 20.

Published in final edited form as:

Biomacromolecules. 2022 December 12; 23(12): 5137–5147. doi:10.1021/acs.biomac.2c00985.

Species-Based Differences in Mechanical Properties, Cytocompatibility, and Printability of Methacrylated Collagen Hydrogels

Sarah M. Ali,
Department of Biomedical and Chemical Engineering and Sciences, Florida Institute of Technology, Melbourne, Florida 32901, United States

Nashaita Y. Patrawalla,
Department of Biomedical and Chemical Engineering and Sciences, Florida Institute of Technology, Melbourne, Florida 32901, United States

Nilabh S. Kajave,
Department of Biomedical and Chemical Engineering and Sciences, Florida Institute of Technology, Melbourne, Florida 32901, United States

Alan B. Brown,
Department of Biomedical and Chemical Engineering and Sciences, Florida Institute of Technology, Melbourne, Florida 32901, United States

Vipuil Kishore
Department of Biomedical and Chemical Engineering and Sciences, Florida Institute of Technology, Melbourne, Florida 32901, United States

Abstract

Collagen methacrylation is a promising approach to generate photo-cross-linkable cell-laden hydrogels with improved mechanical properties. However, the impact of species-based variations in amino acid composition and collagen isolation method on methacrylation degree (MD) and its subsequent effects on the physical properties of methacrylated collagen (CMA) hydrogels and cell response are unknown. Herein, we compared the effects of three collagen species (bovine, human, and rat), two collagen extraction methods (pepsin digestion and acid extraction), and two photoinitiators (lithium phenyl-2,4,6-trimethylbenzoylphosphinate (LAP) and Irgacure-2959 (I-2959)) on the physical properties of CMA hydrogels, printability and mesenchymal stem cell (MSC) response. Human collagen showed the highest MD. LAP was more cytocompatible than I-2959. The compressive modulus and cell viability of rat CMA were significantly higher ($p < 0.05$) than bovine CMA. Human CMA yielded constructs with superior print fidelity. Together, these results suggest that careful selection of collagen source and cross-linking conditions is essential for biomimetic design of CMA hydrogels for tissue engineering applications.

Corresponding Author: Vipuil Kishore – Department of Biomedical and Chemical Engineering and Sciences, Florida Institute of Technology, Melbourne, Florida 32901, United States; vkishore@fit.edu.

The authors declare no competing financial interest.

Complete contact information is available at: https://pubs.acs.org/10.1021/acs.biomac.2c00985

Graphical Abstract

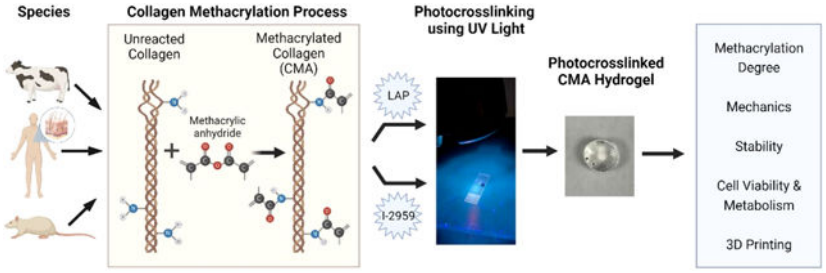

1. INTRODUCTION

Collagen type I, the most abundant protein in the human body, is characterized by a helical triple ring conformation composed of two pro-alpha (a_1) polypeptide chains and one pro-alpha (a_2) chain.[1,2] Each unit of the collagen molecule consists of a repeating glycine-X-Y triplet with X and Y usually representing amino acids proline and hydroxyproline.[3] This structure provides collagen with unique functionality such as biocompatibility, biodegradability, permeability, and fibrillogenesis.[4,5] Collagen's ubiquitous nature, biological characteristics, and ease of processing have allowed for its use in a range of different biomaterial-based applications including grafts and various manufactured products.[6] However, weak mechanical properties and increased susceptibility to enzymatic degradation are major limitations.

To address these limitations, chemical cross-linking schemes with agents such as genipin or carbodiimide (i.e., EDC-NHS) cross-linkers are routinely used to impart mechanical stability to collagen scaffolds.[7,8] However, cytotoxicity of chemical cross-linkers, especially when applied directly to cell-laden scaffolds, is a major concern.[9] For example, Kajave et al. have shown that application of low concentrations of genipin (i.e., 1 mM) directly to human mesenchymal stem cells (MSC) resulted in significant decrease in cell viability.[10] Recent work has shown that it is feasible to modify the chemical structure of the collagen molecule via methacrylation of the free amine groups and yet maintain the innate functionality of the polymer.[11] Methacrylated collagen (CMA) is amenable to photochemical cross-linking in the presence of a cytocompatible photoinitiator and UV light to yield mechanically improved cell-laden collagen hydrogels without loss in cell viability.[11,12] On the basis of prior literature, while methacrylation mainly modifies the ϵ-amine groups, the minority of OH- groups can also be modified, and therefore CMA can also be termed collagen methacryloyl.[13]

Distinct species-based differences exist in the amino acid composition of collagen.[14–17] Because methacrylation of collagen chemically modifies the free amine groups on the collagen backbone, species-based differences in amino acid composition are bound to impact the methacrylation degree (MD) and therefore can also influence the physical properties of CMA as well as the cellular response. In addition, differences in isolation methods (i.e., acid extraction vs enzymatic digestion) yield collagen protein with structural disparities with (telo) and without (atelo) the telopeptide ends which can also impact the

properties of CMA. While prior studies have investigated the effects of different species and isolation techniques on properties of collagen hydrogels,[18–20] how these innate structural differences impact the physiochemical properties of CMA is unknown. In addition, changes in compositional and mechanical properties of CMA can also influence cell behavior and its applicability as a bioink for 3D printing applications. Therefore, there is a need for a systematic investigation to unravel the effects of species and isolation technique-based structural differences of collagen on MD and its subsequent effects on the physical properties and cytocompatibility of CMA. Such knowledge can be vital in selection of appropriate collagen source for the development of biomimetic 3D hydrogels systems and bioinks for tissue engineering applications.[21,22]

In this study, collagen isolated from three different species (i.e., bovine, human, and rat) were modified using the same methacrylation process. Bovine and human collagen were pepsin digested (atelo) whereas rat collagen was isolated via acid extraction (telo). Two different photoinitiators (Irgacure (I-2959) or lithium phenyl-2,4,6-trimethylbenzoylphosphinate (LAP)) were employed for photochemical cross-linking. The effects of different species, isolation method, and photoinitiator type on physical properties, cytocompatibility, and 3D print fidelity of CMA were investigated.

2. MATERIALS AND METHODS

2.1. Materials.

PureCol, bovine hide type I collagen solution, 3.1 mg/mL (bovine), and RatCol, rat tail type I collagen solution, 4 mg/mL (rat), were purchased from Advanced BioMatrix (Carlsbad, CA). HumaDerm, human skin type I collagen lyophilized (human), was purchased from HumaBiologics, Inc. (Phoenix, AZ). Methacrylic anhydride (2000 ppm topanol A as inhibitor, 94%), collagenase (*Clostridium histolyticum*, 1873 U/mL), and 2,4,6-trinitrobenzenesulfonic (TNBS) acid solution (5% w/v) were purchased from Sigma-Aldrich, Inc. (St. Louis, MO). Lithium phenyl-2,4,6-trimethylbenzoylphosphinate (LAP) and Irgacure (I-2959) were also purchased from Advanced BioMatrix (Carlsbad, CA). Deuterium oxide (99.9 atom % D), deuterium chloride for NMR (20 wt % solution in D_2O, 100.0 atom % D), and all other chemicals and reagents were purchased from Fisher Scientific (Waltham, MA) unless stated otherwise.

2.2. Methacrylation of Collagen.

Bovine, human, and rat collagen solutions were first reconstituted to 3.1 mg/mL using 10 mM HCl for bovine and human collagen and 20 mM acetic acid for rat collagen. Each collagen sample was then reacted with sodium phosphate dibasic to make a 0.1 M buffer. Following this, 160 μL of methacrylic anhydride (MA) was added dropwise to 2 mL of collagen solution and reacted for 8 h at 4 °C. Solution pH was maintained between 7 and 7.5 during the first hour following MA addition, using 1 M NaOH for any necessary adjustments. Following the reaction period, excess MA and buffer were removed via centrifugation at 2000*g* at 4 °C, and the supernatant was collected. Collagen solution was then transferred to a 6–8 kDa dialysis tube and dialyzed against 10 mM HCl for 3 days at 4 °C with dialysate changes twice daily. After dialysis, the CMA solution was frozen

at −20 °C and lyophilized. The final product was obtained by solubilizing the lyophilized CMA in 10 mM HCl for bovine and human CMA and 20 mM acetic acid for rat CMA at a concentration of 6 mg/mL for all the experiments.

2.3. Confirmation and Quantification of Methacrylation.

Methacrylation of collagen species was verified using proton nuclear magnetic resonance (^{1}HNMR).[11] A Bruker Avance 400 MHz NMR was used to obtain spectra of both CMA and unmethacrylated collagen for each species at room temperature. NMR samples were prepared by combining freeze-dried CMA from two separate batches and dissolving in deuterated DMSO (3.1 mg/mL). NMR spectra of each species of CMA and unmethacrylated collagen were taken in triplicate (16 scans) and compared to provide qualitative confirmation of derivatization and semi-quantitative assessment of MD. MD was estimated through examination of the CMA spectra and measurement of the methacrylate beta protons (vinylics) of interest at delta-H 5.65–5.25. These methacrylate vinylics were then compared to aromatic protons at delta-H 8.6–7.6 which were present in the spectra of both CMA and unreacted collagen for all species. Because the aromatic rings are not targeted during methacrylation, they were used for normalizing data from each the spectra.

Trinitrobenzenesulfonic acid (TNBS) assay was also used to quantify the MD.[7] Briefly, lyophilized CMA (1 mg) was incubated in 1 mL of 4% (w/v) sodium bicarbonate buffer and 1 mL of freshly prepared 0.5% (v/v) TNBS solution for 2 h at 40 °C. Following incubation, 3 mL of 6 N HCl was added to stop the reaction, and the solution was allowed to incubate for an additional 2 h at 60 °C. The final solution was then diluted 2-fold with ultrapure water to make a total volume of 10 mL, and 150 μL of the solution was added in triplicate into the wells of a clear bottom 96-well plate (Greiner). The absorbance was measured at a wavelength of 345 nm (SpectraMax M2e plate reader, Molecular Devices). The same protocol was performed with unmethacrylated collagen. The number of free ϵ-amine groups in unmethacrylated collagen and CMA was determined by using the following equation.[23,24]

$$\text{no. of free } \epsilon\text{-amine} = \frac{2 \times \text{Abs}_{345\text{nm}} \times 0.01L \times \text{MW}}{1.46 \times 10^4 \times b \times Y}$$

where 1.46×10^4 L/(mol cm) is the molar absorptivity of TNP-lys, 0.01 L is the total volume of the solution, MW is the molecular mass of collagen (300,000 g/mol), b is the cell path length (cm), and Y is the protein weight (0.001 g).

The MD of each species was determined by calculating the percentage of free amine groups remaining in CMA using the following equation:

$$\text{MD}\ (\%) = \left(1 - \frac{\text{no. of free } \epsilon\text{-amine in CMA}}{\text{no. of free } \epsilon\text{-amine in unmethacrylated collagen}}\right) \times 100$$

2.4. Preparation of Photochemically Cross-Linked Methacrylated Collagen Hydrogels.

CMA prepared using collagen isolated from three different species (bovine, human, and rat) was combined with a photoinitiator (LAP or I-2959) and exposed to UV light to prepare the

hydrogels. At first, 5% w/v stock solutions of LAP and I-2959 photoinitiators were prepared individually, in 70% ethanol. Photoinitiator was then added to pH neutralized CMA solution at a concentration of 0.1% w/v. CMA solution was prepared using an 8:1:1 ratio of CMA, 10x PBS, and 0.1 N NaOH and well mixed at 4 °C. Following this, the CMA solution was extruded into rubber washers (7.5 mm diameter, 2.5 mm height) and exposed to UV light (365 nm, 17 mW/cm^2) for 2 min to induce gelation and form the CMA hydrogels.

2.5. Mechanical Assessment of Photochemically Cross-Linked Methacrylated Collagen Hydrogels.

Uniaxial compression tests were performed to determine the mechanical properties of CMA hydrogels. Briefly, CMA hydrogels (N = 10/group) were hydrated in ultrapure water for 1 h, blotted using a KimWipe, and then carefully mounted onto an acrylic stage of a MT G2Micro Tester (CellScale Biomaterials Testing, Waterloo, Canada). Compression tests were performed using a 0.5 mm cantilever beam mounted with a 3 × 3 mm^2 stainless steel platen tip at a constant loading rate of 10 μm/s. The load was employed until 10% displacement of the hydrogel thickness was achieved. Stress–strain curves were then plotted and analyzed to obtain the compressive modulus from the slope of the 0–10% strain region of the stress–strain curve.[25]

2.6. Assessment of CMA Hydrogel Stability Using *In Vitro* Collagenase Assay.

Stability of the photo-cross-linked CMA hydrogels (N = 8/group) was assessed using an *in vitro* collagenase degradation assay.[26] Briefly, hydrogels were prepared and weighed, and their initial mass (W_0) was recorded. The hydrogels were then incubated in 500 μL of collagenase solution (5 U/mL in 0.1 M Tris-HCl buffer and 5 mM $CaCl_2$, pH 7.4) at 37 °C. At hourly intervals, the hydrogels were removed from the collagenase solution, gently blotted, and weighed (W_t). The residual mass of each gel was then calculated using the following equation:

$$\text{residual mass } (\%) = \frac{W_t}{W_0} \times 100$$

2.7. Morphological Assessment of CMA Hydrogels Using Scanning Electron Microscopy (SEM).

SEM was used to assess the topography of freeze-dried CMA hydrogels. The freeze-drying process was employed to reduce specimen distortion and yield highly porous collagen scaffolds.[27] CMA hydrogels were freeze-dried by dipping them in liquid nitrogen for 15 s followed by lyophilization. Following this, hydrogels were mounted on stubs using carbon adhesive discs, sputter-coated with gold, and observed at 100× magnification under SEM (JEOL JSM-6380LV).

2.8. Cell Culture and Encapsulation in Photochemically Cross-Linked CMA Hydrogels.

Human MSCs (Lonza; PT-2501) were seeded onto 75 cm^2 flasks and maintained in a low-glucose Dulbecco's Modified Eagle Medium (DMEM) growth medium supplemented with 10% fetal bovine serum (FBS) and 1% penicillin/streptomycin in 5% CO_2 at 37

°C. Passage-5 cells were used for all the experiments. Cells were encapsulated within the CMA hydrogels (10^5 cells/mL) by adding them to the pH neutralized CMA and photoinitiator mixture prior to gelation. Hydrogels were prepared by pipetting 100 μL of cell containing CMA–photoinitiator solution into individual wells of a 96-well plate (Corning) and cross-linking for 2 min under a UV lamp (17 mW/cm^2) inside the biosafety cabinet. Following cross-linking, cell-laden hydrogels were cultured in alpha-MEM medium (Gibco) supplemented with 10% FBS and 1% penicillin/streptomycin for 7 days.

2.9. Cell Viability and Metabolic Activity in Cell-Laden CMA Hydrogels.

Cell viability was evaluated on days 1 and 7 using live–dead assay (N = 3 hydrogels/group/time point). Cell-laden hydrogels were washed with 1x PBS and stained using 100 μL of a 1:2 ratio mixture of calcein AM and ethidium homodimer at 37 °C for 45 min. The esterase substrate calcein AM (4 mM in DMSO) stains live cells green while ethidium homodimer III (2 mM in DMSO/H_2O) stains dead cells red. Following this, the cell-laden hydrogels were imaged under a fluorescence microscope (Zeiss). Images were then taken (N = 5 images/sample/group/time point), and image assessment was performed to evaluate cell viability by manually counting the number of live and dead cells present in each image using ImageJ (National Institutes of Health, Bethesda, MD).

Alamar Blue assay was used to measure cell metabolic activity of human MSCs encapsulated in the CMA hydrogels (N = 6 hydrogels/group/time point). At days 1, 4, and 7, the cell-laden hydrogels were incubated with 10% Alamar Blue solution at 37 °C for 4 h. After incubation, 100 μL of solution from each well was added in duplicate into individual wells of a clear bottom 96-well plate (Greiner). Fluorescence was measured at an excitation wavelength of 555 nm and an emission wavelength of 595 nm using a SpectraMax M2e plate reader.

2.10. Assessment of Print Fidelity.

The applicability of CMA synthesized using collagen from different species for use as a bioink was compared by printing 3D grid constructs using the freeform reversible embedding of suspended hydrogels (FRESH) method (N = 3 prints/CMA group).[28] CMA inks were prepared by mixing chilled bovine, human, or rat CMA solution (6 mg/mL), NaOH (0.1 N), and 10x PBS in an 8:1:1 ratio with 0.1% w/v LAP in a syringe. The syringe was mounted on to an extrusion-based printer, REGEMAT 3D Bio V1 (Granada, Spain), and the bioink was extruded into the FRESH bath using the parameters described in Table 1. Photochemical cross-linking of CMA constructs was performed post printing by exposing them to UV light for 2 min. The constructs embedded in FRESH were then incubated at 37 °C for 30 min to melt the gelatin support bath and retrieve the printed constructs. The constructs were gently washed in 1x PBS to ensure removal of gelatin and were stained with a red dye to allow for visualization of the constructs. High quality images of the constructs were taken using a Nikon DX 8–55 mm camera (Tokyo, Japan). The thickness of the cross-struts (4 measurements per cross-strut or 8 measurements per printed construct) and the area of the pore size (4 measurements per construct) were measured using ImageJ to assess printability and evaluate print fidelity.

2.11. Statistical Analysis.

Results are expressed as mean ± standard deviation. Each experiment was repeated at least twice to confirm reproducibility, and data were combined to obtain the sample size. Statistical analysis was performed using one-way ANOVA with Tukey post hoc for pairwise comparisons (JMP Pro 14 Statistical Discovery, SAS, Cary, NC). Statistical significance was set at $p < 0.05$.

3. RESULTS

3.1. Species-Based Differences in Collagen Methacrylation Degree.

^{1}HNMR was initially used to confirm functionalization via methacrylation of the three species of collagen. Representative NMR spectra are shown in Figure 1. Spectra revealed distinct differences between unmethacrylated collagen and CMA for all three species. Methacrylate beta protons (vinylics) at delta-H 5.65–5.25 were present only in CMA. Quantitative assessment of MD using ^{1}HNMR was performed by comparing the number of methacrylate beta protons present at the two peaks of interest (delta-H 5.65–5.25) in each species of CMA. This assessment is shown in Figure 2A, where the *y*-axis is representative of the area of the beta-proton signal, as a fraction of the aromatic signal. The highest MD was observed for human CMA compared to bovine and rat CMA (Figure 2A). These results were confirmed using the TNBS assay which showed that the MD of human CMA was significantly higher ($p < 0.05$) at approximately 40% compared to bovine and rat CMA, which showed a MD of around 25% (Figure 2B). In addition, possible differences in the number of free ε-amine groups for unmethacrylated collagen (159±55, 178±41, and 133±7 per mg of collagen for unmethacrylated bovine, human, and rat collagen, respectively) suggest that species-specific variations in starting amine composition may exist. Together, these results indicate that despite application of the same methacrylation protocol, species-based differences in amino acid composition can yield varying MD of collagen.

3.2. Species and Photoinitiator Effects on Stiffness of CMA Hydrogels.

Typical stress vs strain curves for CMA hydrogels synthesized using collagen isolated from different species and cross-linked using either LAP or I-2959 photoinitiators are shown in Figure 3A. Results showed that the compressive modulus of rat CMA hydrogels was significantly higher than both human and bovine CMA irrespective of the photoinitiator used ($p < 0.05$; Figure 3B). In addition, the compressive modulus of human CMA hydrogels was significantly higher ($p < 0.05$) than bovine CMA hydrogels upon cross-linking with LAP photoinitiator. When comparing different photoinitiators, the compressive modulus of bovine CMA hydrogels cross-linked using I-2959 was significantly higher than the ones cross-linked with LAP ($p < 0.05$). Together, these results indicate that rat CMA hydrogels are stiffer than bovine and human CMA hydrogels.

3.3. Species and Photoinitiator Effects on Stability of CMA Hydrogels.

Change in residual mass over a 4 h period revealed that CMA hydrogels cross-linked using LAP photoinitiator degraded slower compared to the ones cross-linked using I-2959 (Figure 4A). Specifically, human LAP CMA hydrogels degraded significantly slower (p

< 0.05) than human I-2959 CMA hydrogels as indicated by ~70% residual mass when cross-linked with LAP as opposed to <50% residual mass with I-2959 cross-linking (Figure 4B). When comparing different species, the rate of degradation was the fastest for rat CMA hydrogels followed by human and bovine CMA hydrogels for both photoinitiators. Specifically, rat CMA hydrogels showed significantly lower residual mass ($p < 0.05$) at around 40% compared to bovine and human CMA hydrogels that showed >60% residual mass when cross-linked with LAP (Figure 4B). Together these results indicate that bovine and human CMA hydrogels exhibit greater enzymatic stability. In addition, LAP yields more stable CMA hydrogels compared to I-2959.

3.4. Assessment of CMA Hydrogel Surface Morphology Using SEM.

Surface topography of all CMA hydrogels exhibited a rough texture with some degree of porosity which can be attributed to the freeze-drying processing technique employed for sample preparation prior to imaging (Figure 5). In addition, fibrous morphology that is typically found in collagen hydrogels was not observed indicating that CMA hydrogels developed in this work do not undergo fibrillogenesis.[29,30] Overall, no visible difference in microstructure was observed, indicating that change in collagen species and photoinitiator type does not impact the surface morphology of CMA hydrogels.

3.5. Species and Photoinitiator Effects on Cell Viability and Metabolic Activity.

The viability of human MSC encapsulated in CMA hydrogels was evaluated using live–dead assay at days 1 and 7. Qualitative assessment of live–dead images revealed that cells exhibited a round morphology at day 1 and an elongated morphology at day 7 on all hydrogels (Figure 6). Higher cell viability was observed in CMA hydrogels cross-linked with LAP photoinitiator compared to I-2959 (Figure 6). In addition, greater cell viability was evident on rat CMA hydrogels. Quantitative assessment of the live–dead images using image analysis confirmed these findings. Cell viability in CMA hydrogels was maintained between days 1 and 7 when cross-linked using the LAP photoinitiator (Figure 7A). On the other hand, use of I-2959 resulted in a decrease in cell viability with time. When comparing the two photoinitiators, cell viability in bovine CMA and rat CMA hydrogels was significantly higher ($p < 0.05$) when cross-linked with LAP compared to I-2959 (Figure 7A). When comparing different collagen species, no difference in cell viability was observed in LAP cross-linked CMA hydrogels. Photo-cross-linking with I-2959 yielded significantly higher ($p < 0.05$) cell viability in rat CMA and human CMA hydrogels compared to bovine CMA hydrogels. Together, these results indicate that rat CMA and human CMA hydrogels better support human MSC viability, and LAP is more cytocompatible than I-2959.

Cell metabolic activity was assessed using Alamar Blue assay at days 1, 4, and 7. Results revealed that LAP photoinitiator was more cytocompatible than I-2959 for all collagen species (Figure 7B). In addition, human MSC metabolic activity was significantly higher ($p < 0.05$) in rat CMA hydrogels compared to bovine CMA hydrogels when LAP was used as the photoinitiator ($p < 0.05$). These results indicate that both species and photoinitiator type impact metabolic activity of human MSC encapsulated in CMA hydrogels.

3.6. Species-Based Effects on CMA Printability.

Qualitative assessment of print fidelity showed that use of bovine CMA and human CMA as inks yielded 3D constructs with print fidelity comparable to the designed 3D mesh model (Figure 8). On the other hand, rat CMA yielded deformed constructs and hence was rendered not printable. Quantitative measurements revealed that constructs printed using human CMA showed significantly finer line width ($p < 0.05$) and significantly greater pore size ($p < 0.05$) compared to bovine CMA (Figure 8). These results indicate that human CMA exhibits the best print fidelity and hence can be used as a viable bioink for 3D printing of collagen constructs.

4. DISCUSSION

Distinct species-based differences exist in the amino acid sequences of collagen.[31,32] Considering these innate species-based differences and the knowledge that methacrylation specifically involves the alteration of these amino acids on the collagen backbone, it is crucial to understand the effects of different collagen species on MD and its subsequent impact on the physical properties and cytocompatibility of CMA. The current study is the first attempt to compare changes in MD of collagen isolated from three different species —bovine, human, and rat—and using two different extraction methods—acid extraction (telo) and enzymatic digestion (atelo)—and correlate the differences in MD with physical properties, cytocompatibility, and printability of CMA hydrogels. In addition, two different photoinitiators (I-2959 and LAP) were also compared.

According to a report by Meyers, amino acid composition in collagen varies based on not only the species but also the tissues from which they are prepared.[6] While the key repeating glycine motif $(Gly\text{-}X\text{-}Y)_n$ is preserved across species, the ratio of the 21 different amino acids that fill the X and Y positions of the triplicate vary widely depending on the collagen source. The methacrylation process actively targets the amino acids with primary free amine side chains (i.e., lysine and arginine) whose concentration may vary between species.[6] Because collagen from bovine hide and human skin were isolated via pepsin digestion (i.e., atelo collagen), the varying MD obtained between these two species (Figure 2) can be directly attributed to the inherent differences in the amino acid composition. For rat tail collagen, apart from differences in amino acid composition, the method of isolation (i.e., acid extraction, telo collagen) can also impact MD.

The working hypothesis of this study was that higher MD would yield better mechanical properties because of greater levels of cross-linking between the modified amine groups on the collagen backbone. In line with this hypothesis, significantly higher compressive modulus of human CMA can be explained by the greater MD of human CMA compared to bovine CMA (Figure 3). However, the hypothesis is not validated with rat CMA hydrogels which showed the highest stiffness despite exhibiting the lowest MD. These results suggest that structural differences in the collagen molecule, depending on the extraction protocol (i.e., enzymatic extraction vs acid extraction), can impact the mechanical properties.[33] Enzymatic extraction (atelo) involves cleavage of the nonhelical region of the alpha 1 (a_1) and alpha 2 (a_2) chains of the collagen molecule called the aminotelopeptides. Conversely, with acid extraction methods (telo) this telopeptide region is left intact. While both types of

collagen have been proven useful for 3D gel synthesis and cell culture, studies have shown that telocollagen produces mechanically stronger hydrogels than atelocollagen possibly due to the presence of higher number of cross-linking sites within the telopeptide region of the collagen molecule.[19,20,34]

The *in vitro* degradation outcomes can help select specific collagen source depending on end use which may require expedited degradation of collagen-based drug delivery vehicles or more sustained degradation of collagen scaffolds to match the regeneration rate of diseased or damaged tissues in the tissue engineering realm. Prior work has shown that change in species can significantly impact the degradation kinetics of collagen.[35] Results from this study agree with prior work which demonstrated that bovine and human collagen were shown to exhibit greater hydrogel stability than other species examined (Figure 4).[18] The extraction method used to obtain the collagen may have influenced these stability results. The initial exposure of rat collagen to acid during the extraction process may have weakened some of the peptide bonds in the collagen molecule, thus making the rat CMA (telo) more susceptible than bovine and human CMA (atelo) to degradation by the action of the collagenase enzyme which targets these same peptides.[36,37]

SEM results for surface morphology showed that the CMA hydrogels are nonfibrous (Figure 5). This finding is contrary to prior work that showed that collagen post methacrylation retains the fiber formation ability upon exposure to physiological conditions.[12] Unlike prior studies, the collagen methacrylation protocol employed in this study does not involve preactivation of the methacrylic acid using carbodiimide (EDC) prior to reaction with collagen. This modified methacrylation process may explain why the fiber formation abilities of CMA in this study were not preserved post methacrylation.[11,38] Prior research has shown that the fibrous architecture of collagen scaffolds (i.e., aligned vs random collagen fibers) can have a profound effect on cell morphology, proliferation, and tissue-specific differentiation.[39,40] In this study, despite the CMA hydrogels being nonfibrous, high cell viability and proliferation demonstrate that these hydrogels are cytocompatible (Figures 6 and 7). More studies are warranted to evaluate species-based effects in EDC preactivated fibrous CMA hydrogels.

Cell viability results revealed that both collagen species and photoinitiator choice significantly impact the viability and metabolic activity of human MSCs encapsulated in CMA hydrogels (Figures 6 and 7). Human MSCs encapsulated in CMA hydrogels cross-linked using LAP demonstrated significantly greater ($p < 0.05$) cytocompatibility than I-2959, which was consistent with previously published reports.[41,42] Species-based differences revealed that rat CMA was more cytocompatible than bovine CMA; a finding consistent with a recent publication that compared different species of collagen.[18] Higher cell viability and metabolic activity in rat CMA hydrogels may be attributed to greater matrix stiffness of rat CMA compared to bovine CMA counterparts.[43]

3D bioprinting is an additive biofabrication methodology that allows for the development of complex biological structures for use in tissue replacement/regeneration applications. Use of collagen as a bioink for 3D bioprinting is highly advantageous to generate scaffolds that mimic the physicochemical properties of native tissues.[44–46] While collagen hydrogels

are inherently weak, modification of collagen structure via methacrylation allows for photochemical cross-linking of the 3D construct post printing and thereby help retain the fidelity of the printed construct.[47] Previous work has shown that it is feasible to print collagenous structures with high print fidelity using low concentrations of CMA bioink and the FRESH printing approach.[10,48] However, the impact of species-based differences in MD on printability of CMA bioinks is unknown. Results from this study show that applicability of collagen as a bioink for 3D printing depends on the tissue source wherein human CMA and bovine CMA yielded printed constructs while rat CMA was not printable (Figure 8). Higher MD of human CMA compared to bovine CMA may allow for more robust cross-linking of the printed construct and thereby yield constructs with better print fidelity. On the basis of the 3D printing results of this study, bovine- and human-derived collagen can be used as bioinks for extrusion-based printing of collagenous constructs for use in ACL reconstruction and skin regeneration applications.[49,50] 3D printing of architecturally complex tissues can be feasible by designing stereolithography (STL) models, and the layer-by-layer fidelity in the microarchitecture of the resultant prints can be quantified using techniques such as SEM and micro-CT.[51–53] Additionally, extrusion-based printing is dependent on the ink's specific shear thinning coefficients which aid in ease of ink ejection and the formation of prints with high structural fidelity following deposition.[54,55] It is likely that the shear-thinning properties of rat collagen may not be conducive to extrusion-based 3D printing, and therefore use of microvalve or inkjet printing methods may be more suitable for the formation of viable rat collagen constructs for tissue engineering applications.[49,50,55,56]

5. CONCLUSIONS

Results from this work demonstrate that collagen species, extraction method, and photoinitiator choice can significantly impact the mechanical properties, cytocompatibility, and printability of CMA hydrogels. Despite using the same methacrylation protocol, human CMA showed significantly greater MD indicating that possible species-based variations in amino acid composition can influence the MD of collagen. While MD was expected to correlate with the measured physical properties of CMA, results from compression testing showed that telocollagen nature of rat CMA may play a more significant role in governing the mechanical properties of CMA hydrogels. Cell-based assays revealed that human MSCs encapsulated in LAP cross-linked rat CMA had significantly greater viability and metabolic activity than bovine CMA potentially because of the stiffer mechanical properties of rat CMA and reduced cytotoxicity of LAP. Finally, human CMA was the most viable bioink for 3D printing of collagen constructs. Although further research is necessary to understand these effects on other species of collagen, results from this study collectively indicate that judicious choice in selection of collagen source and cross-linking conditions is of vital importance for the generation of cell-laden CMA scaffolds.

ACKNOWLEDGMENTS

This study was supported by a grant from National Institutes of Health (NIH 1R15AR071102). The content reported here is solely the responsibility of the authors and does not necessarily represent the official views of the NIH. In addition, authors would like to acknowledge support from the National Science Foundation (CHE 03-42251) for the purchase of the NMR spectrometer.

REFERENCES

(1). di Lullo GA; Sweeney SM; Körkkö J; Ala-Kokko L; San Antonio JD Mapping the Ligand-Binding Sites and Disease-Associated Mutations on the Most Abundant Protein in the Human, Type I Collagen. J. Biol. Chem. 2002, 277 (6), 4223–4231. [PubMed: 11704682]

(2). Yang L; van der Werf KO; Fitié CFC; Bennink ML; Dijkstra PJ; Feijen J Mechanical Properties of Native and Cross-Linked Type i Collagen Fibrils. Biophys. J. 2008, 94 (6), 2204–2211. [PubMed: 18032556]

(3). Walimbe T; Panitch A Best of Both Hydrogel Worlds: Harnessing Bioactivity and Tunability by Incorporating Glycosaminoglycans in Collagen Hydrogels. Bioengineering 2020, 7, 1–24.

(4). Dong C; Lv Y Application of Collagen Scaffold in Tissue Engineering: Recent Advances and New Perspectives. Polymers 2016, 8 (2), 42. [PubMed: 30979136]

(5). Wolf K; Alexander S; Schacht V; Coussens LM; von Andrian UH; van Rheenen J; Deryugina E; Friedl P Collagen-Based Cell Migration Models in Vitro and in Vivo. Semin Cell Dev Biol. 2009, 20, 931–941. [PubMed: 19682592]

(6). Meyer M Processing of Collagen Based Biomaterials and the Resulting Materials Properties. Biomed. Eng. Online 2019, 18 (1), 24. [PubMed: 30885217]

(7). Alfredo Uquillas J; Kishore V; Akkus O Genipin Crosslinking Elevates the Strength of Electrochemically Aligned Collagen to the Level of Tendons. J. Mech Behav Biomed. Mater. 2012, 15, 176–189. [PubMed: 23032437]

(8). Yang C Enhanced Physicochemical Properties of Collagen by Using EDC/NHS-Crosslinking. Bull. Mater. Sci. 2012, 35 (5), 913–918.

(9). MacAya D; Ng KK; Spector M Injectable Collagen-Genipin Gel for the Treatment of Spinal Cord Injury: In Vitro Studies. Adv. Funct. Mater. 2011, 21 (24), 4788–4797.

(10). Kajave NS; Schmitt T; Nguyen TU; Kishore V Dual Crosslinking Strategy to Generate Mechanically Viable Cell-Laden Printable Constructs Using Methacrylated Collagen Bioinks. Mater. Sci. Eng., C 2020, 107, 110290.

(11). Gaudet ID; Shreiber DI Characterization of Methacrylated Type-I Collagen as a Dynamic, Photoactive Hydrogel. Biointerphases 2012, 7 (1–4), 25. [PubMed: 22589068]

(12). Jongprasitkul H; Turunen S; Parihar VS; Annurakshita S; Kellomäki M Photocross-Linkable Methacrylated Polypeptides and Polysaccharides for Casting, Injecting, and 3D Fabrication. Biomacromolecules 2021, 22 (2), 481–493. [PubMed: 33350816]

(13). Yue K; Trujillo-de Santiago G; Alvarez MM; Tamayol A; Annabi N; Khademhosseini A Synthesis, Properties, and Biomedical Applications of Gelatin Methacryloyl (GelMA) Hydrogels. Biomaterials 2015, 73, 254–271. [PubMed: 26414409]

(14). Schmitt T; Kajave N; Cai HH; Gu L; Albanna M; Kishore V In Vitro Characterization of Xeno-Free Clinically Relevant Human Collagen and Its Applicability in Cell-Laden 3D Bioprinting. J. Biomater Appl. 2021, 35 (8), 912–923. [PubMed: 32957839]

(15). Lin YK; Liu DC Comparison of Physical-Chemical Properties of Type I Collagen from Different Species. Food Chem. 2006, 99 (2), 244–251.

(16). Techatanawat S; Surarit R; Suddhasthira T; Khovidhunkit SOP Type I Collagen Extracted from Rat-Tail and Bovine Achilles Tendon for Dental Application: A Comparative Study. Asian Biomed 2011, 5 (6), 787–798.

(17). Robinson JJ Comparative Biochemical Analysis of Sea Urchin Peristome and Rat Tail Tendon Collagen. Comp. Biochem. Physiol. B, Biochem. 1997, 117 (2), 307–313.

(18). Baltazar T; Kajave NS; Rodriguez M; Chakraborty S; Jiang B; Skardal A; Kishore V; Pober JS; Albanna MZ Native Human Collagen Type I Provides a Viable Physiologically Relevant Alternative to Xenogeneic Sources for Tissue Engineering Applications: A Comparative in Vitro and in Vivo Study. J. Biomed. Mater. Res. B Appl. Biomater 2022, 110 (10), 2323–2337. [PubMed: 35532208]

(19). Maher MK; White JF; Glattauer V; Yue Z; Hughes TC; Ramshaw JAM; Wallace GG Variation in Hydrogel Formation and Network Structure for Telo-, Atelo-and Methacrylated Collagens. Polymers 2022, 14 (9), 1775. [PubMed: 35566947]

(20). Slyker L; Diamantides N; Kim J; Bonassar LJ Mechanical Performance of Collagen Gels Is Dependent on Purity, A1/A2 Ratio, and Telopeptides. J. Biomed. Mater. Res. A 2022, 110 (1), 11–20. [PubMed: 34236763]

(21). Bian L Functional Hydrogel Bioink, a Key Challenge of 3D Cellular Bioprinting. APL Bioeng 2020, 4 (3), 030401. [PubMed: 32743233]

(22). Ruedinger F; Lavrentieva A; Blume C; Pepelanova I; Scheper T Hydrogels for 3D Mammalian Cell Culture: A Starting Guide for Laboratory Practice. Appl. Microbiol. Biotechnol. 2015, 99, 623–636. [PubMed: 25432676]

(23). Ofner CM III; Bubnis WA Chemical and Swelling Evaluations of Amino Group Crosslinking in Gelatin and Modified Gelatin Matrices. Pharm. Res. 1996, 13 (12), 1821–1827. [PubMed: 8987078]

(24). Bubnis WA; Ofner CM The Determination of ϵ-Amino Groups in Soluble and Poorly Soluble Proteinaceous Materials by a Spectrophotometrie Method Using Trinitrobenzenesulfonic Acid. Anal. Biochem. 1992, 207 (1), 129–133. [PubMed: 1489085]

(25). Worthington KS; Wiley LA; Bartlett AM; Stone EM; Mullins RF; Salem AK; Guymon CA; Tucker BA Mechanical Properties of Murine and Porcine Ocular Tissues in Compression. Exp. Eye Res. 2014, 121, 194–199. [PubMed: 24613781]

(26). Omobono MA; Zhao X; Furlong MA; Kwon CH; Gill TJ; Randolph MA; Redmond RW Enhancing the Stiffness of Collagen Hydrogels for Delivery of Encapsulated Chondrocytes to Articular Lesions for Cartilage Regeneration. J. Biomed. Mater. Res. A 2015, 103 (4), 1332–1338. [PubMed: 25044419]

(27). Lee JTY; Chow KL SEM Sample Preparation for Cells on 3D Scaffolds by Freeze-Drying and HMDS. Scanning 2012, 34 (1), 12–25. [PubMed: 22532079]

(28). Hinton TJ; Jallerat Q; Palchesko RN; Park JH; Grodzicki MS; Shue HJ; Ramadan MH; Hudson AR; Feinberg AW Three-Dimensional Printing of Complex Biological Structures by Freeform Reversible Embedding of Suspended Hydrogels. Sci. Adv. 2015, 1 (9), No. e1500758. [PubMed: 26601312]

(29). Exposito JY; Valcourt U; Cluzel C; Lethias C The Fibrillar Collagen Family. Int. J. Mol. Sci. 2010, 11, 407–426. [PubMed: 20386646]

(30). Kadler KE; Holmes DF; Trotter JA; Chapman JA Collagen Fibril Formation. Biochem. J. 1996, 316, 1–11. [PubMed: 8645190]

(31). Piez KA; Eigner EA; Lewis MS The Chromatographic Separation and Amino Acid Composition of the Subunits of Several Collagens*. Biochemistry 1963, 2 (1), 58–66.

(32). Bernstein FC; Koetzle TF; Williams GJB; Meyer EF; Brice MD; Rodgers JR; Kennard O; Shimanouchi T; Tasumi M The Protein Data Bank: A Computer-Based Archival File for Macromolecular Structures. J. Mol. Biol. 1977, 112 (3), 535–542. [PubMed: 875032]

(33). Sato K; Ebihara T; Adachi E; Kawashima S; Hattori S; Irie S Possible Involvement of Aminotelopeptide in Self-Assembly and Thermal Stability of Collagen I as Revealed by Its Removal with Proteases. J. Biol. Chem. 2000, 275 (33), 25870–25875. [PubMed: 10851240]

(34). Nakamura Y Structure of Type I Collagen Dimers. Int. J. Biol. Macromol. 1987, 9 (5), 281–290.

(35). Vallecillo-Rivas M; Toledano-Osorio M; Vallecillo C; Osorio R; Toledano M The Collagen Origin Influences the Degradation Kinetics of Guided Bone Regeneration Membranes. Polymers 2021, 13 (17), 3007. [PubMed: 34503047]

(36). Daboor SM; Budge SM; Ghaly AE; Brooks S-L; Dave D Extraction and Purification of Collagenase Enzymes: A Critical Review. Am. J. Biochem Biotechnol 2010, 6 (4), 239–263.

(37). Chung L; Dinakarpandian D; Yoshida N; Layer-Fields JL; Fields GB; Visse R; Nagase H Collagenase Unwinds Triple-Helical Collagen Prior to Peptide Bond Hydrolysis. EMBO J. 2004, 23 (15), 3020–3030. [PubMed: 15257288]

(38). Drzewiecki KE; Parmar AS; Gaudet ID; Branch JR; Pike DH; Nanda V; Shreiber DI Methacrylation Induces Rapid, Temperature-Dependent, Reversible Self-Assembly of Type-i Collagen. Langmuir 2014, 30 (37), 11204–11211. [PubMed: 25208340]

(39). Kishore V; Bullock W; Sun X; van Dyke WS; Akkus O Tenogenic Differentiation of Human MSCs Induced by the Topography of Electrochemically Aligned Collagen Threads. Biomaterials 2012, 33 (7), 2137–2144. [PubMed: 22177622]

(40). Taufalele PV; VanderBurgh JA; Munoz A; Zanotelli MR; Reinhart-King CA Fiber Alignment Drives Changes in Architectural and Mechanical Features in Collagen Matrices. PLoS One 2019, 14 (5), No. e0216537. [PubMed: 31091287]

(41). Xu H; Casillas J; Krishnamoorthy S; Xu C Effects of Irgacure 2959 and Lithium Phenyl-2,4,6-Trimethylbenzoylphosphinate on Cell Viability, Physical Properties, and Microstructure in 3D Bioprinting of Vascular-like Constructs. Biomed. Mater. 2020, 15 (5), 55021.

(42). Fairbanks BD; Schwartz MP; Bowman CN; Anseth KS Photoinitiated Polymerization of PEG-Diacrylate with Lithium Phenyl-2,4,6-Trimethylbenzoylphosphinate: Polymerization Rate and Cytocompatibility. Biomaterials 2009, 30 (35), 6702–6707. [PubMed: 19783300]

(43). Bachmann B; Spitz S; Schädl B; Teuschl AH; Redl H; Nürnberger S; Ertl P Stiffness Matters: Fine-Tuned Hydrogel Elasticity Alters Chondrogenic Redifferentiation. Front Bioeng Biotechnol 2020, 8, 373. [PubMed: 32426347]

(44). Marques CF; Diogo GS; Pina S; Oliveira JM; Silva TH; Reis RL Collagen-Based Bioinks for Hard Tissue Engineering Applications: A Comprehensive Review. J. Mater. Sci.: Mater. Med. 2019, 30 (3), 32. [PubMed: 30840132]

(45). Osidak EO; Kozhukhov VI; Osidak MS; Domogatsky SP Collagen as Bioink for Bioprinting: A Comprehensive Review. Int. J. Bioprint 2020, 6, 1–10.

(46). Stepanovska J; Otahal M; Hanzalek K; Supova M; Matejka R Ph Modification of High-Concentrated Collagen Bioinks as a Factor Affecting Cell Viability, Mechanical Properties, and Printability. Gels 2021, 7 (4), 252. [PubMed: 34940312]

(47). Zennifer A; Manivannan S; Sethuraman S; Kumbar SG; Sundaramurthi D 3D Bioprinting and Photocrosslinking: Emerging Strategies & Future Perspectives. Mater. Sci. Eng., C 2021, 137, 112576.

(48). Kajave NS; Schmitt T; Nguyen TU; Gaharwar AK; Kishore V Bioglass Incorporated Methacrylated Collagen Bioactive Ink for 3D Printing of Bone Tissue. Biomed. Mater. 2021, 16 (3), 035003.

(49). Kajave NS; Schmitt T; Patrawalla NY; Kishore V Design-Build-Validate Strategy to 3D Print Bioglass Gradients for Anterior Cruciate Ligament Enthesis Reconstruction. Tissue Eng. Part C Methods 2022, 28 (4), 158–167. [PubMed: 35357966]

(50). Jiao T; Lian Q; Lian W; Wang Y; Li D; Reis RL; Oliveira JM Properties of Collagen/Sodium Alginate Hydrogels for Bioprinting of Skin Models. J. Bionic Eng. 2022, 1–14.

(51). Trachtenberg JE; Placone JK; Smith BT; Fisher JP; Mikos AG Extrusion-Based 3D Printing of Poly(Propylene Fumarate) Scaffolds with Hydroxyapatite Gradients. J. Biomater Sci. Polym. Ed 2017, 28 (6), 532–554. [PubMed: 28125380]

(52). Hockaday LA; Kang KH; Colangelo NW; Cheung PYC; Duan B; Malone E; Wu J; Girardi LN; Bonassar LJ; Lipson H; Chu CC; Butcher JT Rapid 3D Printing of Anatomically Accurate and Mechanically Heterogeneous Aortic Valve Hydrogel Scaffolds. Biofabrication 2012, 4 (3), 035005. [PubMed: 22914604]

(53). Zhang J; Eyisoylu H; Qin XH; Rubert M; Müller R 3D Bioprinting of Graphene Oxide-Incorporated Cell-Laden Bone Mimicking Scaffolds for Promoting Scaffold Fidelity, Osteogenic Differentiation and Mineralization. Acta Biomater 2021, 121, 637–652. [PubMed: 33326888]

(54). Paxton N; Smolan W; Böck T; Melchels F; Groll J; Jungst T Proposal to Assess Printability of Bioinks for Extrusion-Based Bioprinting and Evaluation of Rheological Properties Governing Bioprintability. Biofabrication 2017, 9 (4), 044107. [PubMed: 28930091]

(55). Ramesh S; Harrysson OLA; Rao PK; Tamayol A; Cormier DR; Zhang Y; Rivero I. v. Extrusion Bioprinting: Recent Progress, Challenges, and Future Opportunities. Int. J. Bioprint 2021, 21, No. e00118.

(56). Lee JM; Suen SKQ; Ng WL; Ma WC; Yeong WY Bioprinting of Collagen: Considerations, Potentials, and Applications. Macromol. Biosci 2021, 21 (1), 2000280.

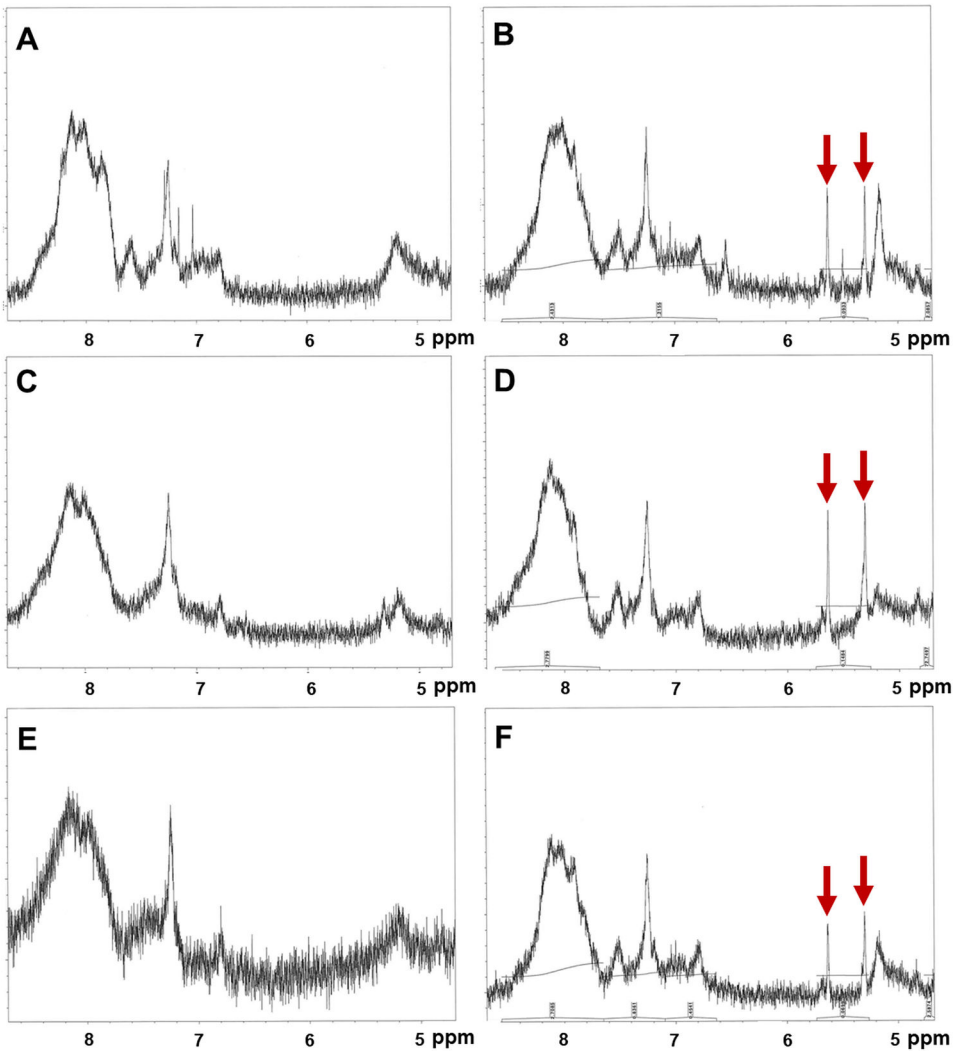

Figure 1.

NMR spectra of unmethacrylated (A) bovine, (C) human, and (E) rat collagen. NMR spectra of methacrylated (B) bovine, (D) human, and (F) rat collagen. Red arrows denote the presence of methacrylate beta protons.

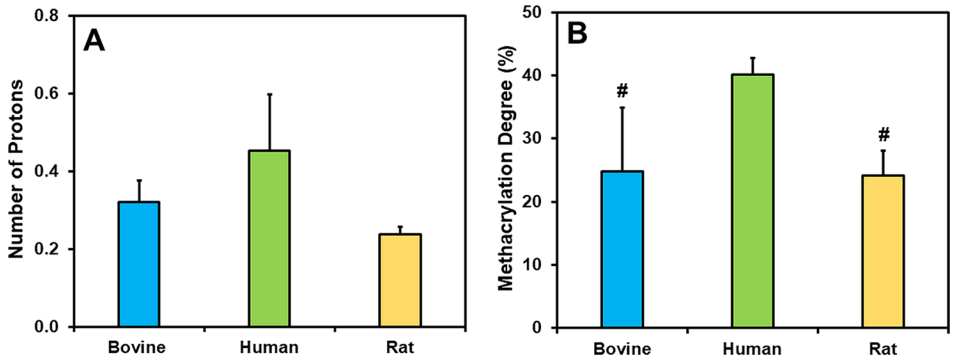

Figure 2.

(A) Quantification of beta-protons from NMR spectra of bovine, human, and rat CMA. (B) Quantification of MD using TNBS assay (# denotes $p < 0.05$ compared to human CMA).

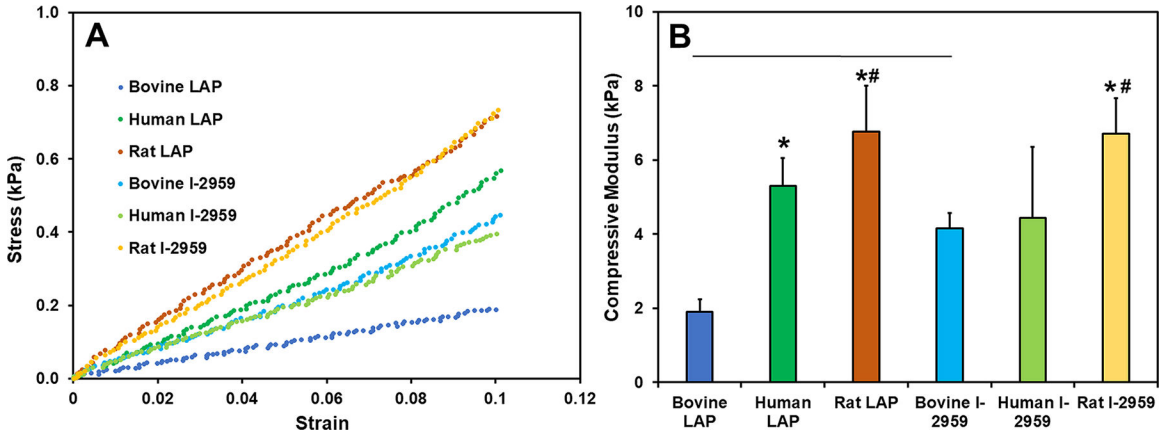

Figure 3.

(A) Representative stress vs strain curves of CMA hydrogels. (B) Compressive modulus of CMA hydrogels (* denotes $p < 0.05$ compared to bovine CMA, # denotes $p < 0.05$ compared to human CMA, and horizontal line denotes $p < 0.05$ between connecting groups indicating photoinitiator-based differences).

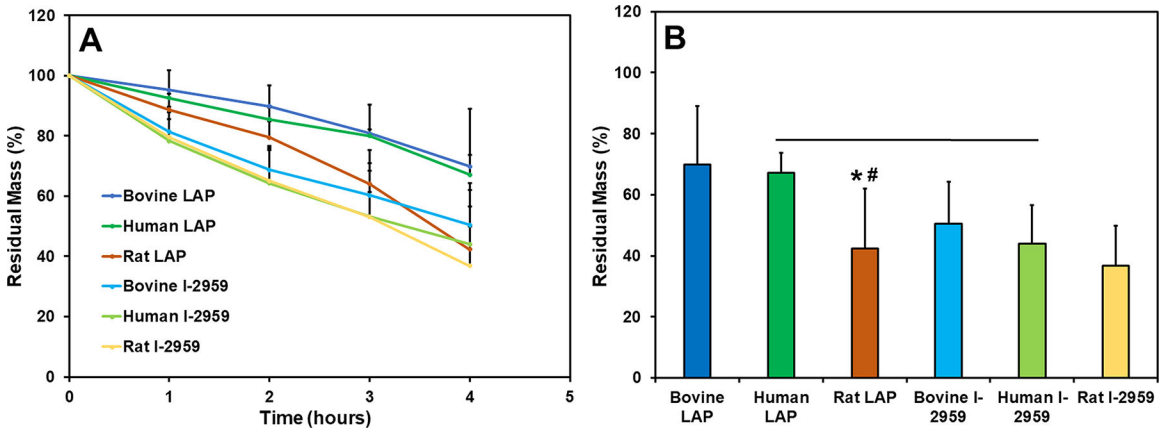

Figure 4.

(A) Degradation kinetics of CMA hydrogels for assessment of stability using *in vitro* collagenase degradation assay. (B) Residual mass of CMA hydrogels at 4 h time point (* denotes $p < 0.05$ compared to bovine CMA, # denotes $p < 0.05$ compared to human CMA, and horizontal line denotes $p < 0.05$ between connecting groups indicating photoinitiator-based differences).

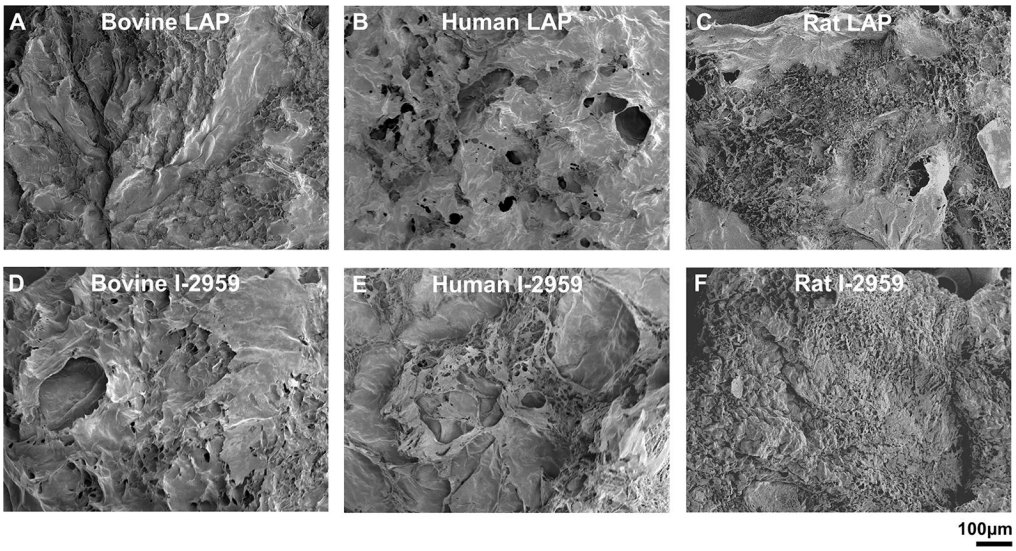

Figure 5.
Assessment of surface microstructure of CMA hydrogels using SEM.

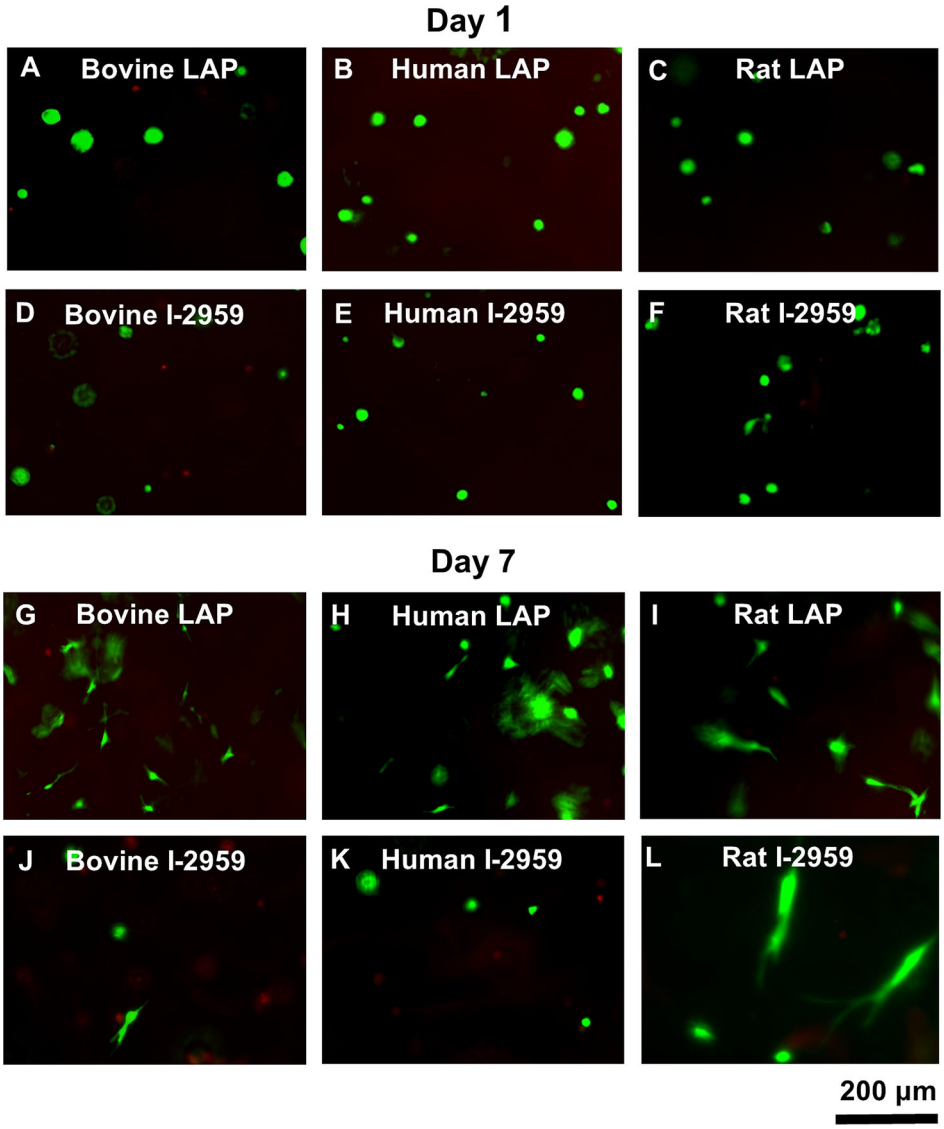

Figure 6.

Live–dead assay to assess viability of human MSC encapsulated in CMA hydrogels at day 1 (A–F) and day 7 (G–L).

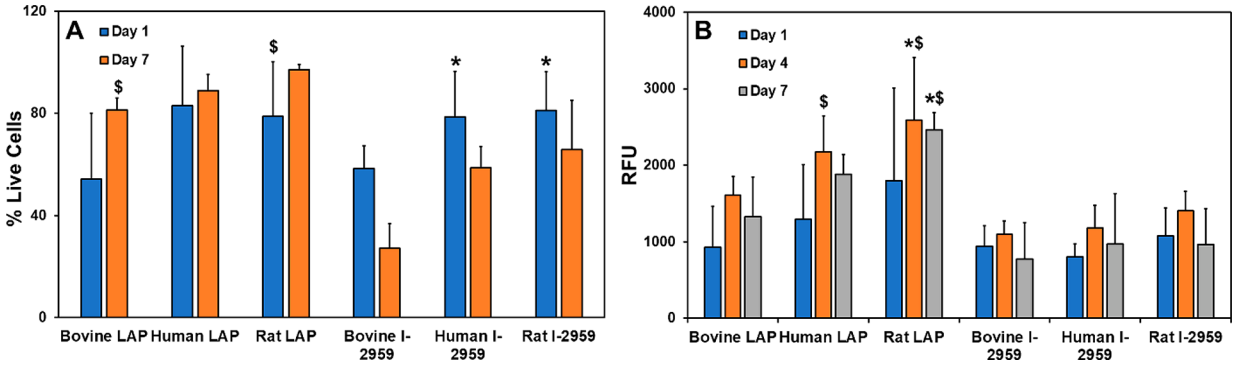

Figure 7.

(A) Quantification of cell viability of human MSCs encapsulated in CMA hydrogels using live–dead assay. (B) Assessment of cell metabolic activity using Alamar Blue assay (* denotes $p < 0.05$ compared to bovine CMA, # denotes $p < 0.05$ compared to human CMA, and $ denotes $p < 0.05$ compared to I-2959 for the same species and time point of comparison).

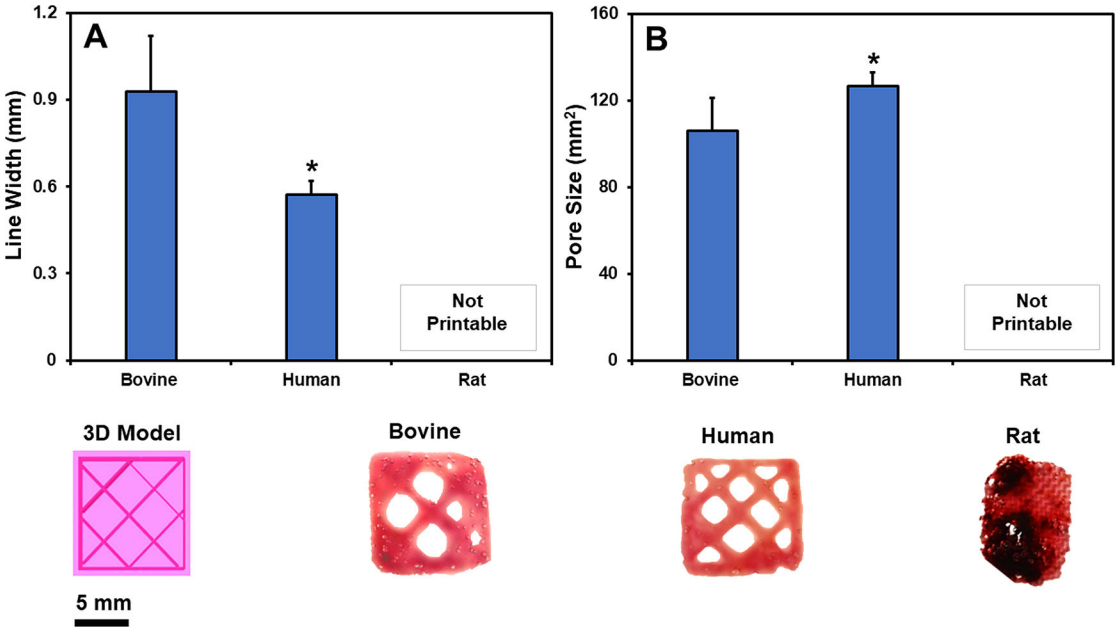

Figure 8.

Print fidelity of 3D printed CMA constructs as compared to the original model. Assessment of (A) line width and (B) pore size of 3D printed CMA constructs (* denotes $p < 0.05$ compared to bovine CMA).

Table 1.

Parameters for 3D Printing of CMA Constructs

parameter	value	description
tip diameter	0.25 mm	a blunt 25 gauge syringe tip for bioink extrusion
print shape	cube	10 mm × 10 mm × 1 mm cube
infill pattern	mesh	cross-hatched inner patter
infill angle	45°	extrusion angle within the construct
flow speed	5 mm s^{-1}	extrusion speed
cross-link power	17 mW cm^{-2}	power of the UV light
cross-linking duration	2 min	exposure time to UV light